Technical Report

Unreacted Shock and Detonation Response of EXP-A Measured with Embedded Electromagnetic Gauges

David Lacina, Ben Wilde*, and Christopher Neel***
*Air Force Research Laboratory, Munitions Directorate, Eglin AFB, FL
**University of Dayton Research Institute, Eglin AFB, FL

01 October 2020

1 ABSTRACT

Embedded electromagnetic (EM) particle velocity gauges have been used to characterize the unreacted shock and detonation response of EXP-A, an RDX-based explosive material under development by the Air Force. To study the shock and detonation response, a sustained 1D planar shock wave (>2 µsec pulse duration) was imparted into the EXP-A using gun launched flyer plates, achieving pressures up to 11.2 GPa. The embedded electromagnetic gauges recorded (in-situ) time-resolved particle velocity traces which were used to determine Hugoniot (unreacted shock velocity and pressure) and Pop-plot (shock-to-detonation distance/time) information. The Hugoniot for EXP-A is well-described by U_S=1.25 *km/s* + 3.32*u_P, and the shock-to-detonation distance (X_D) is best described by $Log_{10}(X_D)$=2.02-1.47*Log_{10}(Pressure). Results from short pulse (~200-300 ns pulse duration) initiation experiments are also outlined and compared to the sustained pulse (>2 µsec) results.

2 INTRODUCTION

In recent years, there has been a steady improvement in the experimental techniques used to characterize the shock response of energetic materials. Such information is crucial for the development of accurate reactive flow/burn models, which are used to predict material response and improve weapon design.[1,2] In this work, an embedded electromagnetic (EM) gauge diagnostic[3,4,5] was employed to measure, in-situ, the unreacted shock and detonation behavior of EXP-A. EXP-A is of interest because it is an inexpensive RDX-based energetic material that possesses the higher performance (e.g. Gurney energy) of an HMX-based energetic. To ensure that a weapon system performs as expected, existing data from other energetic materials can't be confidently used in design models in place of information for the actual explosive of interest. Therefore, the Air Force has undertaken a focused effort to characterize EXP-A, as well as other energetic materials,[2] with the ultimate objective of parameterizing a predictive reactive flow model (e.g., Ignition & Growth model).

Density can strongly influence shock sensitivity of an explosive material.[6] For example, density variations of 0.004-0.007 g/cc can alter the shock-to-detonation distance of PBX-9501 up to 17%,[4] However, density variations (i.e. porosity) have been found to have the greatest effect on the Hugoniot.[7] This is based on an examination of the effect of porosity, and other parameters, on the initiation behavior of many pure and composite explosives.[7] Modelling efforts can take such variations, and their effects, into account using initiation measurements from the same material at different densities, or by using approximations based upon measurements obtained from the material of interest as well as similar energetics.

In terms of explosive initiation, the time dependence of the shock that drives an energetic toward detonation is critical. For instance, a sustained pulse shock (a few μs or longer), a short pulse shock (a few 100ns or shorter), or an explosively-driven shock can lead to successful initiation of an energetic, but all result in very different initiation criteria. The criteria used to describe the initiation of an energetic material is energy (i.e. duration of high pressure state) and power (i.e. pressure).[6] For sustained pulse shocks, the long duration of the pulse renders the energy essentially infinite, as far as initiation phenomena are concerned, and so the initiation of the energetic becomes a function of pressure alone. This is usually reported as a Pop-plot in logarithmic space, which shows the shock-to-detonation distance of the energetic as a function of the input shock pressure.[6] Initiation of an energetic using a short pulse shock is a function of both energy and pressure. For example, a short pulse shock inducing the same pressure state (i.e. power) as a sustained pulse shock will possess lower energy for initiation, due to the shorter duration of shock. In such cases, the James criteria,[8,9] which utilizes both time dependent energy and time dependent power terms in its equations, is used to describe the initiation conditions.

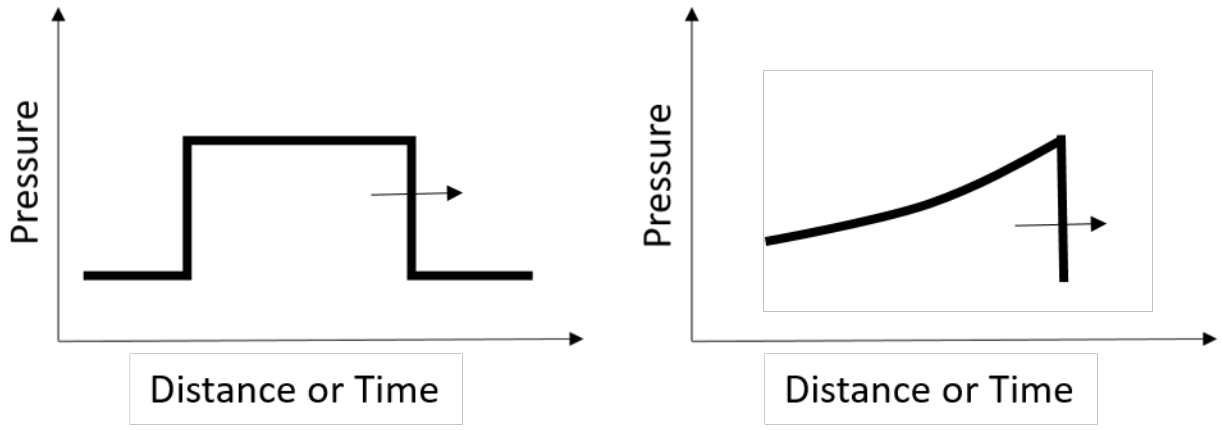

Figure 1. Left: waveform of a sustained or short pulse shock, and Right: waveform of an explosively-driven shock.

Both of the previously outlined shock initiation techniques differ from explosively driven shocks, where the pressure loading takes the form of a triangle wave (Figure 1).[10,11] Unlike the square wave form of a sustained or short pulse shock, a triangular loading wave introduces a peak pressure state in the subject material which decays over time.[10,11] This instability in the pressure makes it difficult to identify the exact pressure state at the time of initiation. As such, the pressure used to describe initiation would be an average value whose accuracy depends on the time dependent reduction of the pressure, which is dependent on the experimental configuration.[10,11] The degree to which energy would be an issue depends on how significant and rapid this time dependent pressure reduction was. This would affect the uncertainty of any acquired Pop-plot data, and could potentially lead to disagreements with sustained or short pulse initiation data.

For the reasons stated above, the shock-to-detonation distance at any specific pressure, plus other critical weapon design parameters, can vary depending on the shock loading method (i.e. sustained, short, or explosively driven) used for initiation.[1,2] There have been many efforts to obtain initiation characteristics of energetic materials using either explosively driven[2,7,12,13] or sustained pulse shocks.[4,14,15,16,18] However, there have been few efforts to use large diameter impactors to obtain initiation data using both sustained and short pulse shocks.[15,16] Neel et. al.[17] has addressed this issue for EXP-A, using the data presented in this work along with additional data using short pulse shocks. That work also explores the differences in short pulse shock initiation criteria obtained using gun-driven, large diameter flyers with explosively-driven, small diameter flyers. For the purpose of initiation criteria, sustained pulse shocks resulting from gun-driven flyers or explosively-driven flyers are generally considered to have the same characteristics, as long as the pulse duration is sufficiently long ($\sim>1\mu s$).[11]

Since weapon design and initiation are inherently limited within weaponized configurations, and an initiation system can employ any of the aforementioned types of shock pulses, it is critical to understand the initiation characteristics of any energetics being used in such systems across the widest possible input conditions. Furthermore, understanding initiation characteristics over a wide range of input conditions is useful in predicting the response of a weaponized configuration to unintentional stimuli.

One of the primary methods for characterizing the initiation and detonation behavior of an energetic material is the embedded electromagnetic gauge technique.[1,4,14,15,16,18] The embedded electromagnetic gauge technique was developed and refined over the past 50 years by numerous researchers at several institutions, most notably Los Alamos National Lab.[3,4,5] This is-situ measurement diagnostic, which relies on embedding a film containing electrical wires into the sample itself, works on the principle of electromagnetic induction. A voltage is created as embedded electrical wires move, due to passage of a compression wave, through an externally-applied magnetic field. The induced voltage measurements are converted to particle and shock (or detonation) velocity using knowledge of the magnetic field strength, the geometrical configuration,

and electrical conditions of the experiment.[3,4] Embedded electromagnetic gauges which capture unreacted shock and detonation information in real time (in-situ) has many advantages. For instance, minimal perturbation of the shock and the ability to acquire more information (e.g. particle velocity wave profiles) than other diagnostics (e.g. traditional wedge test) that obtain similar data.[1,16]

Although the use of embedded electromagnetic gauges has increased in recent years, much of the initiation information for energetic materials has been obtained using traditional wedge tests.[2,7,12,13] This is also true for EXP-A (ρ=1.63 g/cc), where explosively driven shocks have been recently used to characterize shock sensitivity (i.e. Pop-plot).[19] This report contains the following: 1) embedded electromagnetic gauge experiments to obtain the unreacted shock (i.e. Hugoniot) and detonation properties of EXP-A initiated by a sustained pulse shock, and 2) unreacted shock (i.e. Hugoniot) and detonation properties of EXP-A initiated by a short pulse shock (<200-300 ns), and 3) an analysis of the shock and detonation response variability induced by density variation and by different pressure loading methods.

3 EXPERIMENTAL DETAILS

3.1 Material

The material that was investigated in this work is EXP-A (89% RDX and 11% LMA [lauryl methacrylate] binder system). EXP-A is a cast cure explosive (i.e. poured into molds for curing) that was prepared at the High Explosive Research and Development facility at the Air Force Research Lab. The molds used to produce the samples for these EM gauge experiments consisted of a set of large molds and a set of small molds, so that the resulting castings were ready for assembly into the final cylindrical-shaped sample, as described later (Figure 2).

The density of each sample was determined by taking its mass and dividing by its volume, calculated using detailed measurements of the large and small castings dimensions. The average density of the material used in these experiments was found to be 1.604 ± 0.004 g/cc. The TMD for this material is 1.64 g/cc, resulting in an average porosity of ~2.2%. The longitudinal acoustic, transverse, and bulk sound speeds have not been measured for EXP-A, but are expected to be measured at some point in the future.

The impactor materials used in this work were high purity alumina (Coorstek, 99.9%),[20] yttria-stabilized tetragonal zirconia polycrystal (Refractron inc., 99.7% purity),[21] and Polychlorotetraflouroethylene (PCTFE, KEL-F81).[22] All materials have been well-characterized and their relevant properties are listed below in Table 1.

Table 1. Equation of State parameters used in impedance matching calculations.

Material	Density	Thickness	Hugoniot Curve	Valid Press. Range
YTZP	6.08 g/cc	9.7 mm	$U_S=7.085-0.08202*u_p + 5.712*u_p^2$	0-16 GPa
Alumina	3.88 g/cc	10.2 mm	10.74 km/s $U_S=12.16-12.55*u_p+14.73*u_p^2$	Elastic: 0-5.7 GPa 5.7-14 GPa
KEL-F81	2.14 g/cc	1.185 mm	$U_S=2.03+1.68*u_p$	

3.2 Embedded Electromagnetic Particle Velocity Gauging

Particle velocity wave profiles were measured using embedded electromagnetic (EM) gauging that has been developed by Los Alamos National Lab.[3,4,5] Figure 2a illustrates a typical embedded gauge experiment. The gauge package used in this study, shown in Figure 2b, consists of twelve ~5μm thick aluminum gauge elements, encapsulated between two layers of ~25μm thick fluorinated ethylene propylene (FEP) Teflon. Nine gauge elements at different depths in the material are used to measure particle velocity history (#1-9 in Figure 2b) and three shock trackers (left tracker, right tracker, and center tracker in Figure 2b) are used to determine the shock velocity from the shock wave arrival times at different material depths.

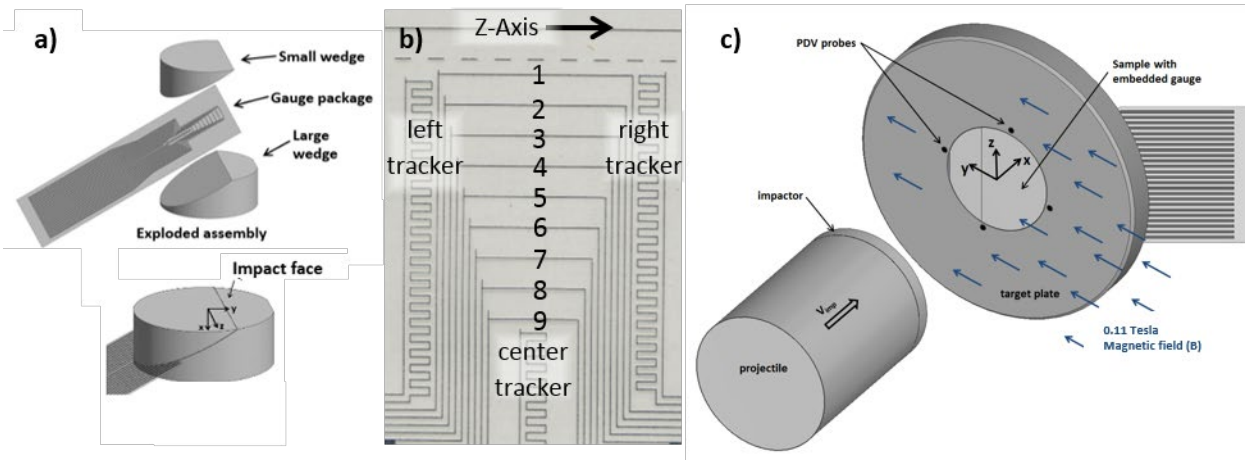

Figure. 2. Experimental setup. (a) Exploded view of the embedded gauge sample and the final assembled target. (b) Image of gauge elements in the gauge package that is embedded in samples (c) The target mounted sample in Fig. 2a is shown in the experimental orientation. The magnetic field lines (along the y-axis), the embedded gauge elements (along the z-axis), and direction of motion due to impact (along the x-axis) are mutually orthogonal.

The methodology associated with this technique has been described in more detail elsewhere.[3,4] Briefly, the sample is manufactured as two castings, shown in Figure 2a. The angled surface, which the gauge package is bonded to, is machined to a 30° angle. This places the individual gauges at different depths in the sample. The impact face of the assembled sample is machined flat while keeping the 30° angle of the gauge package. The sample is then mounted and aligned to the launch tube and magnetic field at the gun muzzle, inside a magnet capable of producing a uniform magnetic field. The gauges produce particle velocity information via Faraday's Law:

$$V_G = L \cdot u_P \times B \quad (1)$$

V_G is the voltage generated by the gauge motion in a uniform magnetic field, L is the gauge length of each embedded EM gauge (typically measured prior to sample/target assembly, varying from 0.5-1.5 cm), B is the magnetic field strength measured at the gauge region, and u_P is the particle velocity of the gauge. The experimental geometry is designed so that the orientation of the gauges, the magnetic field, and the direction of material motion are mutually orthogonal to reduce Faraday's law (Eqn. 1) to a scalar equation: $V_G = Lu_PB$.

There are four conditions which must be met to use the scalar form of Eqn. 1 during analysis. First, the magnetic field (B) near the gauge region must be spatially uniform during the measurement so that B can maintain a scalar value and not be a vector with spatial dependence. Second, the magnetic field (B) must be temporally uniform during the measurement to prevent B from becoming a variable with time dependence. Thirdly, the material (particle) velocity is uniform in the region around the active gauge elements and the gauge film and conductive traces, whose response is actually being measured, moves with the surrounding material. Fourth, that the gauge elements, B field, and material motion (u_p) are mutually orthogonal to reduce the vector operators in eqn. 1 (e.g. the cross product) to scalar operators. If the gauges, B field, and material motion are not mutually orthogonal, then the vector equation must be used in the analysis.

3.3 Experimental Setup

Impactors were accelerated to desired velocities using a 60mm single-stage powder gun.[23] The relative orientation of the projectile/impactor, target plate, and magnetic field is shown in Figure 2c. The EXP-A sample was epoxied into an acrylic target plate and mounted at the gun muzzle, inside a Helmholtz coil electromagnet which generates a ~0.11 Tesla field (B in eqn. 1) in the y direction. All experimental components (i.e. projectile, impactor, target plate, etc.) were non-conductive to maintain the temporal stability of the magnetic field during an experiment. The magnet was positioned to ensure spatial uniformity of the magnetic field in the gauge region of the sample, and the field strength was measured immediately prior to each experiment.

Electrical self-shorting pins, at the rear surface of the explosive samples (not shown), were used to trigger diagnostics. Four non-metallic PDV probes arrayed closely around the central hole of the acrylic target plate, to see the edge of the incoming projectile, measured projectile velocity and impact time using a "traditional" PDV system.[24] The projectile velocity was taken as the average of the four values immediately prior to impact, which typically agreed within ~0.1%. Tilt of the impactor surface at contact was <5mrad, determined using the projectile-PDV probe impact times. To improve the PDV light return, the impact surfaces of the impactors were coated (via vacuum deposition) with aluminum.

The Hugoniot state for these EM gauge experiments, specifically the input pressure (P) and sample particle velocity (u_p), was determined by impedance matching using the initial density of the sample (ρ_0), the measured projectile velocity (V_{imp}), the experimentally determined unreacted

shock velocity (described later), and the known Hugoniot curves for the impactor materials (Table 1).[10] The particle velocity for a detonating explosive material can't be determined directly from the recorded particle velocity traces because the material velocity behind the shock front increases with shock propagation distance (Figure 3a).

3.4 Experimental Results

Figure 3 displays an example of the data obtained from electromagnetic gauge measurements after analysis. The displayed traces have been generated by using Equation 1. Arrival times were assigned to each particle velocity gauge (corresponding to 50% of the rise), as well as to every step on the shock trackers. The time origin was the impact time determined from the PDV probe measurements. The embedded gauge arrival times were then plotted against the known depths (x in the coordinate system of Figure 2c) of each gauge to generate an x-t plot, shown in Figure 3b.

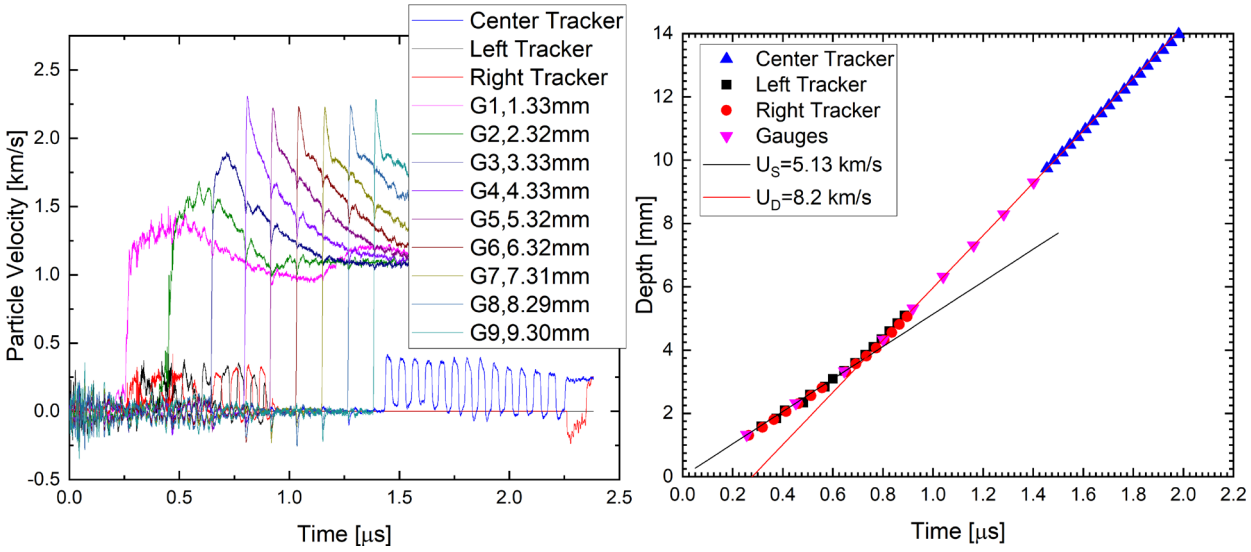

Figure 3. Example of post-analysis embedded EM gauge data for shot FY19-19 (a) Particle Velocity vs Time and (b) Depth vs. Time.

The arrival times for each gauge increase linearly with depth, changing in slope at a transition point known as the shock-to-detonation distance, or just "run distance", (X_D). At earlier times, the shock wave progresses through the material at the shock velocity (U_S) that is determined by the unreacted (inert) material Hugoniot. At later times, beyond X_D, a detonation wave moves through the material at the explosive-specific detonation velocity (D), which is faster than U_S. Each set of gauge/tracker datapoints, either before or after X_D, is fit to a line. The different sets of fitted parameters are then averaged to obtain the slope of the fitted line, which is reported as the measured shock velocity or detonation velocity. Both of these fits can be seen in Figure 3b as the black and red lines, and the run distance is their intersection point (X_D =3.61mm).

The expected Chapman-Jouget (or CJ) state particle velocity for the detonating explosive can be estimated using:

$u_{p,CJ}=D^*(1-0.7125\rho_o^{0.04})$ (Cooper, Explosive Engineering pg.265).[6] (2)

Since detonation velocities for the sustained pulse experiments varied from 8.17-8.25 km/s, the $D_{average}$=8.22 km/s. Using this value with a density (ρ_o) of 1.604 g/cc, equation 2 indicates that $u_{p,CJ}$=2.25 km/s. This agrees with the peak particle velocity observed in Figure 3, as well as the particle velocity traces for other EM gauge experiments which are not shown.

Seven embedded EM gauge experiments were performed on the explosive material. Particle velocities, type of shock pulse used, shock velocities, input pressures, and shock-to-detonation distances are listed in Table 2. The sustained pulse experiments used impactors (Tables 1 and 2) of a thickness sufficient to impart a shock wave into the test material which lasted several microseconds.[10] The impactors for the short pulse shock experiments (Tables 1 and 2) were thinner so that the release from the back of the impactor would limit the duration of the shock that was initially input into the sample to ~200-400 ns. The short pulse shock is continuously attenuated by the higher velocity rarefaction wave as the short pulse shock moves through the material.[10]

Table 2. Measured Shock and Detonation Parameters from embedded electromagnetic gauge experiments

Shot ID	Impactor	Shock Pulse	V_{imp}	U_S	X_D	u_p	P
			km/s	km/s	mm	km/s	GPa
FY19-17	YTZP	Sustained	1.518	5.48 ±0 .080	2.93 ± .200	1.2707 ± .003	11.17±0.13
FY19-18	Alumina	Sustained	1.249	4.74 ± 0.072	5.05 ± .204	1.0508 ± .006	7.99 ± 0.08
FY19-19	YTZP	Sustained	1.389	5.13 ± 0.074	3.61 ± .202	1.1723 ± .003	9.65 ± 0.12
FY19-20	Alumina	Sustained	0.967	4.05 ± 0.066	8.41 ± .210	0.8391 ± .002	5.44± 0.08
FY20-12	Kel-F81	Short	2.145	4.95 ± 0.400	4.81 ± .404	1.086 ± .033	8.62 ± 0.41
FY20-13	Kel-F81	Short	1.502	3.88 ± 0.200	>10	0.7890 ±.016	4.91 ± 0.16
FY20-15	Kel-F81	Short	1.583	4.01 ± 0.100	>10	0.8275±.008	5.32 ± 0.10

The uncertainty in either the shock or detonation velocity was determined as the standard deviation of the U_S or D value after averaging the fitted lines. The uncertainty in the shock-to-detonation distance is the uncertainty in the transition point determination, which largely depends on the uncertainty in the shock velocity. The uncertainty in the shock velocity is dominated by the uncertainty in the impactor tilt. This is because the slope of the fitted line that is used to determine shock velocity is a combination of the effects of both the material shock velocity and of a tilted shock. Gun launched flyers always impart a shock that is tilted to some degree into the samples studied in these types of experiments. To subtract out the effect of a tilted shock, corrections are made to the shock-gauge arrival times based upon the measured tilt, but any uncertainty about the impactor tilt will directly impact that correction. Other contributors to uncertainty in the shock velocity are typically small in these experiments and so are not discussed. To determine the uncertainty in the particle velocity, a 2% uncertainty in the pressure from the impactor Hugoniot

was applied, carrying the uncertainty in U_s through the impedance matching calculations, and assuming no uncertainty in projectile velocity.[25]

Figure 3 shows that there is an unusual degree of signal noise in the tracker traces at early times, which then disappears at later time. The particle velocity traces for all FY19 experiments (Table 2) exhibit this elevated signal noise, but not the FY20 experiments (which were short-pulse shocks using different impactors). Also, this noise only seems to exist in the timeframe where the EXP-A is under shock compression and has not yet detonated. Once the sample is detonating, the signal noise goes away. Since this noise disappears at different depths and times, corresponding to the detonation transition point for the individual experiments, this noise would seem to be caused by some property of the EXP-A itself. A possible explanation can be found in embedded gauge results published on composition B by LANL.[18] Noise in their pre-detonation (i.e. buildup to detonation) particle velocity traces was observed and ultimately attributed to a localized piezoelectric effect in the RDX crystals. It is possible that something similar is happening in this work on EXP-A, and that it might not be seen in the FY20 experiments due to the different shock loading conditions.

4 DISCUSSION OF SUSTAINED PULSE EXPERIMENTS

4.1 Hugoniot

Figure 4 shows the unreacted shock velocities and pressures for EXP-A under sustained pulse shock loading (~>2μs) as a function of particle velocity and volume, respectively. The Hugoniot is shown in both U_S-u_p space and P- V space.

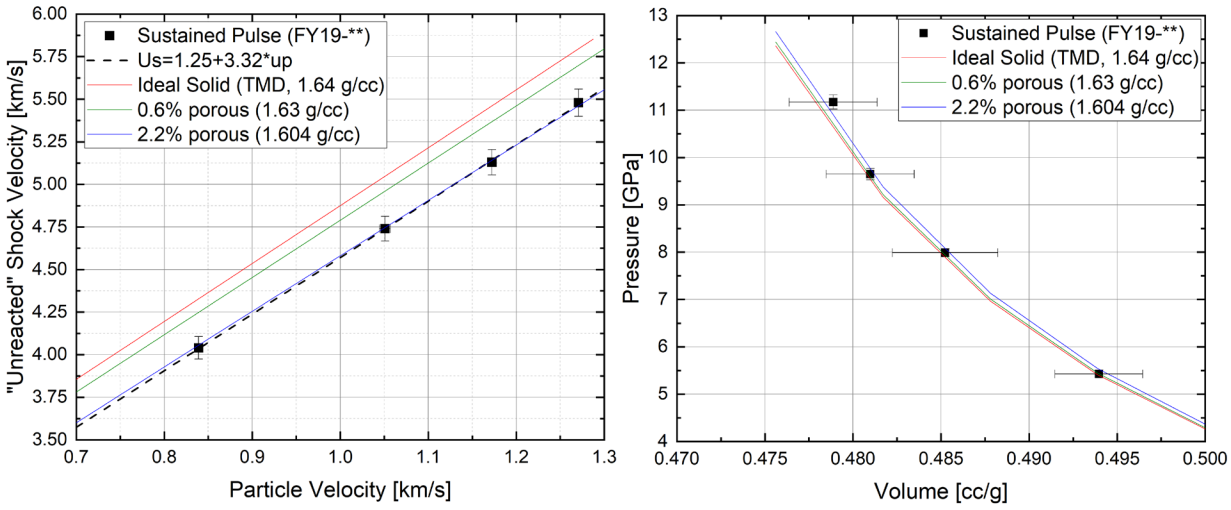

Figure 4. (Left) Particle Velocity (u_p) vs. Unreacted Shock Velocity (U_S) data for EXP-A and (Right) Pressure vs. Volume (in linear space) for EXP-A. Us-u_p plot shows the fit to the data from equation 3 (dashed line). Also shown is the anticipated effect of porosity (i.e. density variation) on the Hugoniot and P-V data, calculated using McQueen compaction model.[26] Estimated fits for the ideal solid (red), 0.6% porosity (green), and 2.2% porosity (blue) are shown.

A linear fit is sufficient to characterize the U_S-u_p trend of the sustained pulse shock data:

$$U_S=1.25+3.32*u_p \text{ km/s}, \quad (3)$$

All of the data points shown in Figure 4a agree very well with this linear fit, within 0.5%. Error bars illustrate the shock velocity uncertainty, which is relatively low and determined as described previously. The particle velocity uncertainty in the Hugoniot data points is low enough that the error bars cannot be easily seen in Figure 4a.

As mentioned previously, density variation can strongly influence the shock and detonation response of an energetic material.[4,7] In an effort to estimate the effect that density might have on the Hugoniot curve of EXP-A, the porous compaction method of McQueen[26] has been used to scale the Hugoniot fit in Figure 4a based on varying porosities (i.e. densities). In this approach, a linear fit for the ideal solid was adjusted until the fit for 2.2% porosity, or a density of 1.604 g/cc, aligned with the acquired EXP-A data in both U_S-u_p and P-V space. The good agreement between this fit and equation 3 is seen in Figure 4a as the blue and dashed black lines, respectively. The fit for 0.6% porosity (density=1.63 g/cc) was also calculated and displayed. These calculations indicate that the fully dense Hugoniot for this material is $U_S=1.47+3.4*u_p$, and at 0.6% porosity is $U_S=1.43+3.36*u_p$.

4.2 Shock-to-detonation Transition

The sustained pulse shock-to-detonation transition distances of EXP-A were determined using the previously described analysis methods. Shock-to-detonation distances were extracted from each of the sustained pulse experimental datasets and then plotted in linear and logarithmic space, shown in Figure 5. A power law fit to the sustained pulse shock data is:

$$\text{Log}_{10}(X_D)=2.02-1.47*\text{Log}_{10}(\text{Pressure}). \quad (4)$$

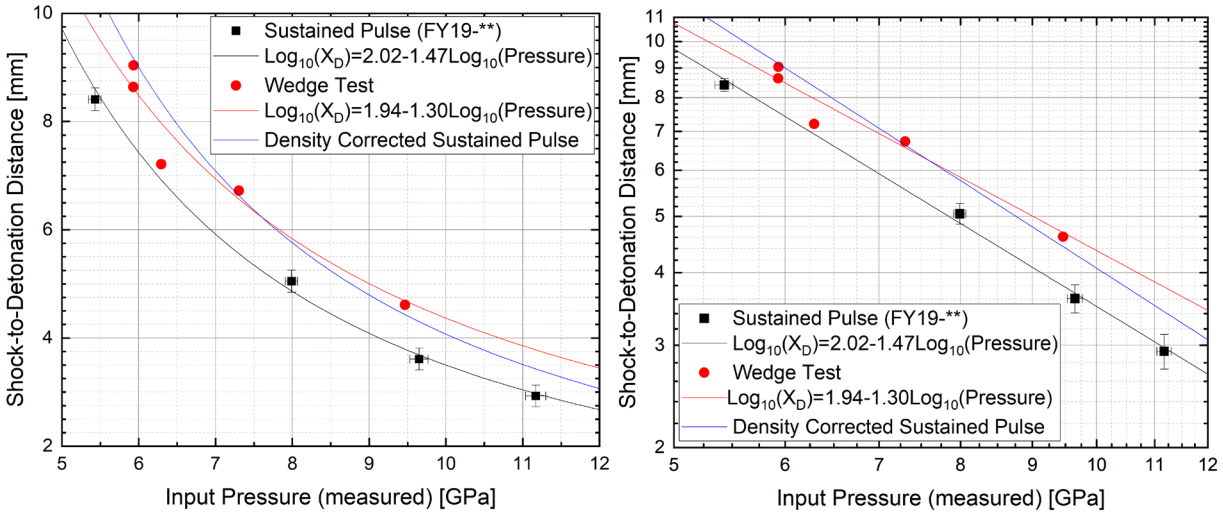

Figure 5. Pressure vs. Shock-to-detonation distance data for EXP-A on a (Left) linear scale and (Right) logarithmic scale. EM gauge test data and power law fit shown in black. Wedge test data and power law fit shown in red. The impedance matching method was used to determine input pressures for both sets of data. Density corrected sustained pulse fit (1.604 g/cc to 1.63 g/cc) is shown in blue.

For comparison purposes, sensitivity data for EXP-A that was obtained from traditional wedge tests[19] is also shown in Figure 5. The power law fits illustrated in Figure 5 agree with their respective data sets fairly well, except for one of the wedge test data points. The EM gauge data and wedge test data seem to be relatively close, but the EXP-A used in the EM gauge experiments appears to have been more sensitive than that used in the wedge tests. Two explanations for this sensitivity variation are the density difference in the tested material and the variation resulting from different testing methods.

The density of the wedge test samples was 1.63 g/cc, compared to 1.604 g/cc for the material studied in this work. The explanation for the density difference is that they were made in separate batches using separate processes. The previous section illustrated that density variation affects the Hugoniot, but such variation also affects the sensitivity. This is because a lower density energetic material has more pores than the same material at higher density. Higher porosity leads to a greater degree of pore collapse under pressure loading and subsequent hot spot formation. More numerous, larger volume hot spots will enhance the initiation of an energetic material.

To understand the degree that these density variations might have on the sensitivity of EXP-A, the measured EM gauge sensitivity data was scaled to match the higher density wedge test data. A pressure dependent correction factor was determined by analyzing Pop-plot datasets taken from PBX-9404 at different densities, at 1.72g/cc and 1.84g/cc.[13] This data was chosen due to the general similarity of HMX and RDX materials and a lack of similar data at different densities for an RDX based material. The result of this analysis was the following equation: $\alpha(P)_{PBX\text{-}9404}$=2.21-

0.53(Log(P)). This describes $X_D(\rho=1.84) = \alpha(P)*X_D(\rho=1.72)$ for PBX-9404. Taking the density difference between the wedge test and EM gauge test EXP-A (0.026g/cc) as a percentage of the difference in the PBX-9404 correction (~21.7% of 0.12 g/cc) results in a correction of [1+(α(P)-1)*0.217]. Using this equation to correct the embedded gauge data to match the wedge tests data produces the blue line in Figure 5. Although the slope of the corrected fit differs from the actual wedge test data, the degree of the shift induced by the density correction appears to agree. This would suggest that the sensitivity differences between the two tests is largely due to the density variation and these results illustrate the degree that density variation affects the sensitivity of EXP-A. However, this analysis is only meant to estimate the potential effect density variation would have on the sensitivity of this material and is not meant to be definitive. More experiments and more rigorous analysis is needed to obtain quantitative conclusions.

The effect of density does not preclude the role that different testing methods can have on producing different sensitivity measurements, which is known to be an issue.[1,11] Partly, this is due to differences in analysis methodology, but some is due to the nature of the input shock used to load the sample. The wedge tests referenced in this work utilized explosively driven shocks. As mentioned previously, the pressure state imparted into a sample by an explosively driven (triangle) shock wave is not the same as a sustained pulse or short pulse (square) wave, largely being an average of the time dependent decay of the pressure state. Based on CTH calculations of the wedge test experimental setup, it is likely that the pressure value for the wedge tests could decrease up to a maximum of ~0.25 GPa.[19] Although the actual pressure drop in the reaction zone is likely to be less than this value, it is still a contributing factor in the variation observed in Figure 5.

5 DISCUSSION OF SHORT PULSE EXPERIMENTS

5.1 Hugoniot

The short pulse shock experiments, and analysis, were carried out in the same manner as the sustained pulse data described earlier. The only differences between the short pulse experiments and the sustained pulse experiments were the thickness and material of the impactors. Using thinner impactors creates a competition between a short pulse shock which initiates the energetic and a faster rarefaction wave from the rear of the impactor which attenuates the shock pulse. Gustavsen at al.[16] has suggested that the energetic will not initiate if the rarefaction wave attenuates the shock before the required shock-to-detonation distance for a particular pressure.

The particle velocity traces for the short pulse shock experiments were more difficult to analyze with the linear fitting method employed in this work, partly related to the different input conditions. Figure 6a shows the Hugoniot fit and data from Figure 5a with the short pulse shock data (blue triangles) added. The short pulse shock data was not used in determining the linear Hugoniot fit in Figure 5a due to the higher uncertainty associated with the short pulse results. However, the short pulse shock experimental results (FY20-12, FY20-13, and FY20-15) shown in Figure 6a agree with the trends established by the sustained pulse results.

The greater uncertainty in the FY20-12 and FY20-13 data points was dominated by uncertainty in the shock velocity determination. FY20-12 data was of poor quality, with most of the tracker data unreadable. This presented few points for the linear fit of the x-t plot, resulting in a larger uncertainty in the slope of the x-t plot fitted line (linear) that provides the shock velocity. FY20-13 had higher than normal uncertainty associated with the impactor tilt value. As mentioned previously, uncertainty regarding the impactor tilt translates to shock velocity uncertainty due to the effect it has on the (tilted shock) corrections that are performed during analysis.

For FY20-13 and FY20-15, the Lagrangian release wave speed could be determined from the unloading visible in the EM gauge traces, shown in Figure 6a (green diamonds).[25] The release wave speeds for FY20-13 and FY20-15 was C_L = 4.95± 0.05 km/s and C_L = 5.06± 0.05 km/s, respectively. The release wave speed couldn't be determined from the other sustained pulse and short pulse shock experimental data because of the presence of the build up to detonation, which obscured the unreacted release wave in the particle velocity traces.

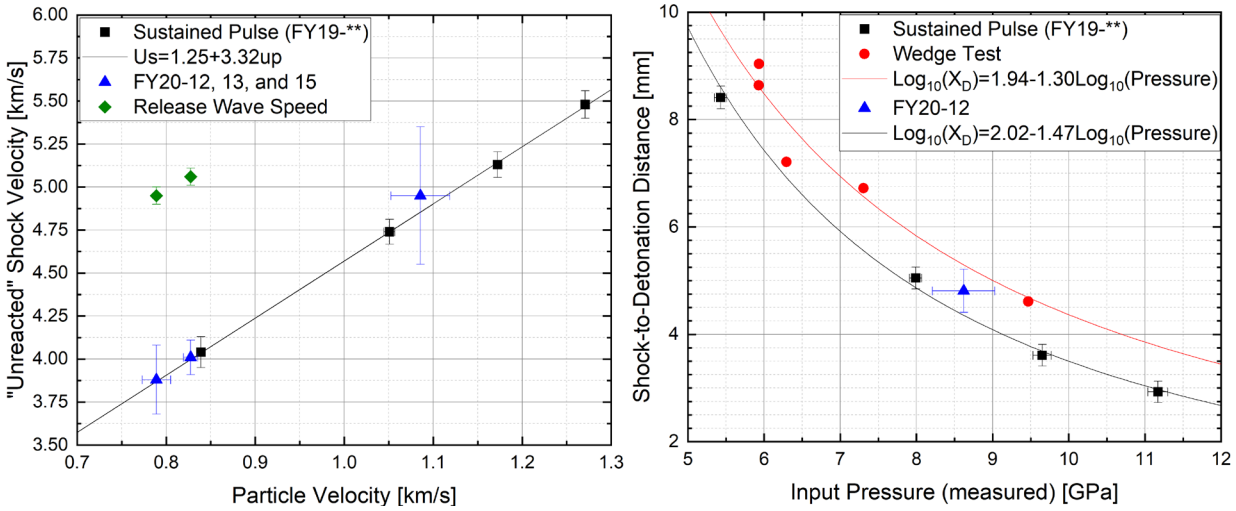

Figure 6. (Left) Particle Velocity (u_p) vs. Unreacted Shock Velocity (U_S) data for EXP-A (Right) Pressure vs. Shock-to-detonation distance data for EXP-A. The U_S-u_p plot shows the sustained pulse shock data and linear fit (black line) from Figure 4a, the datapoints from the short pulse shock experiments (blue triangles), and the calculated release wave speeds (green diamonds). The P- X_D plot shows the data and fits from Figure 5a, with the addition of the short pulse data (blue triangle).

5.2 Shock-to-detonation Transition

The shock-to-detonation data from FY20-12, shown in Figure 6b, falls in line with both test series and is considered consistent with the displayed sustained pulse shock data. The difference observed between the sustained and short pulse shock data is believed to be due to complications caused by short pulse shock initiation that arises under certain circumstances. The offset observed in 6b is evidence of these complications, as are the absence of initiation data for the other two short pulse shock experiments. Based on the sustained pulse results in Figures 5 and 6, the shock-to–

detonation distances for FY20-13 and FY20-15 should have been observable within the timeframe that the experimental data was acquired. In both cases they were still building to detonation at distances well beyond where initiation was anticipated.

For short pulse shocks, it has been previously observed that the shock-to-detonation distance increases as the pulse duration shortens,[15] and that the shock-to-detonation distance is the same for short pulse and sustained pulse initiation provided the short pulse duration is long enough.[8,9,27] As mentioned earlier, short pulse shocks will be a square wave (in P vs. time) until either building to detonation or until the higher velocity rarefaction wave attenuates it. The attenuation of the short pulse shock pushes the material to the threshold that separates initiation from quenching. As the material comes increasingly closer to this initiation threshold, the shock-to-detonation distance and preceding buildup will become progressively longer than for sustained pulse shocks at the same pressure. If the short pulse shock duration is too short, then it will be fully attenuated before reaching the shock-to-detonation distance, quenching the reaction. Conversely, a longer duration short pulse shock, where attenuation does not significantly affect it, leads to a shock-to-detonation distance that will be close to, or match, sustained pulse results. A detailed discussion of this concept, including a method to estimate shock-to-detonation distance when short pulse shocks drive EXP-A close to the initiation threshold, will be provided in a separate EXP-A publication.[17]

SUMMARY

A series of embedded electromagnetic (EM) gauge experiments were performed to characterize the unreacted shock and detonation response of EXP-A, an RDX-based energetic material, using gun launched flyer plates. The experimental test series covered pressures from 5-11.2 GPa to allow for the Hugoniot (unreacted shock velocity and pressure) and the Pop-plot (shock-to-detonation distance/time) to be determined over a wide range of initiation conditions. Impedance matching was used to determine the particle velocity in the EXP-A, utilizing those measurements.

The acquired Hugoniot data followed a linear trend while the shock-to-detonation results were fit to a standard Pop-plot power law relationship. The effect of density variation (i.e. porosity) on the Hugoniot was estimated by using McQueen's porous compaction method.[26] The effect of density variation on the sensitivity data of EXP-A was determined through a comparison with unpublished wedge test data (ρ=1.63 g/cc)[19] and by scaling the sustained pulse EM gauge data, using datakm for PBX-9404 which had been acquired at different densities.[13] In comparison to the wedge tests results for EXP-A, the shock-to-detonation distances were lower for the EM gauge results. This is sensible as the samples studied in the EM gauge tests were lower density and should therefore be more shock sensitive due to the correlation between porosity and hot spot formation.

Results from short pulse (~200-300 ns) initiation experiments were also outlined and compared to the sustained pulse (>2 μs) results mentioned above. The Hugoniot and sensitivity results largely agree between the different pressure loading methods. Differences in the sensitivity results are likely due to the different input conditions associated with short pulse shocks (i.e. energy and

power). This response behavior was briefly explored, with a greater discussion to be carried out in future publications.

6 APPENDIX

FY19-17

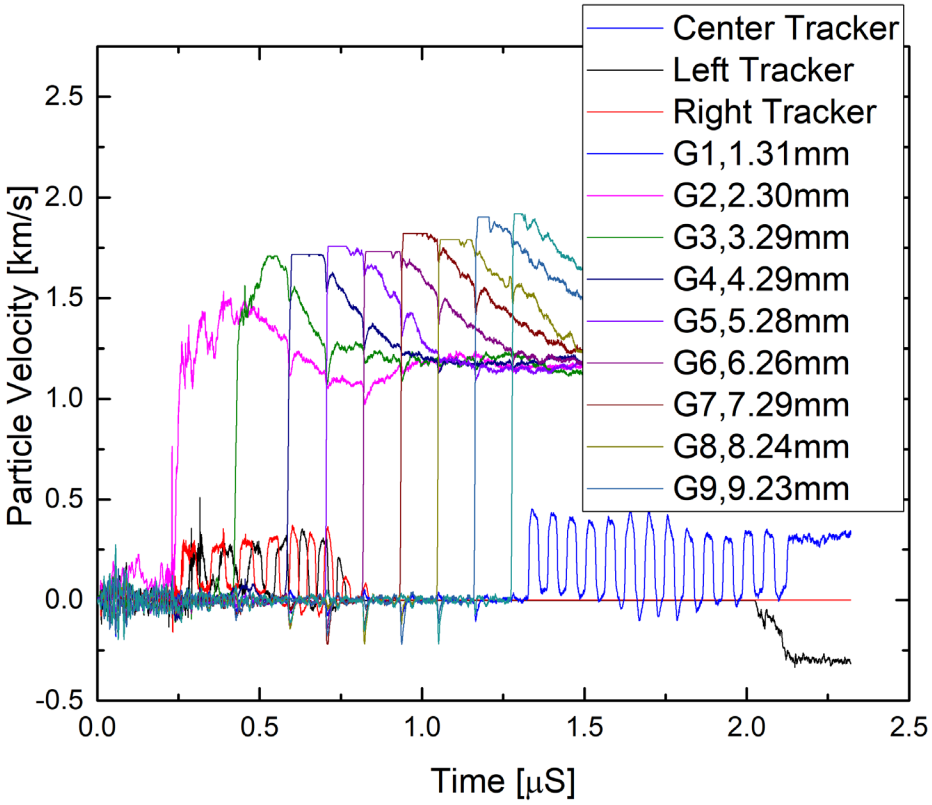

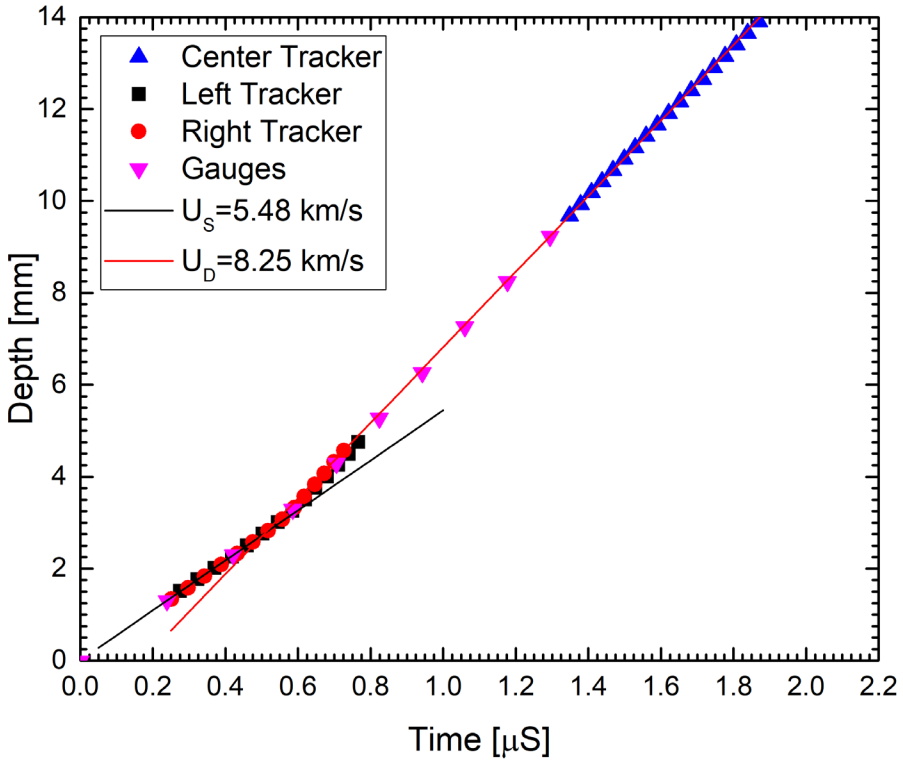

FY19-18

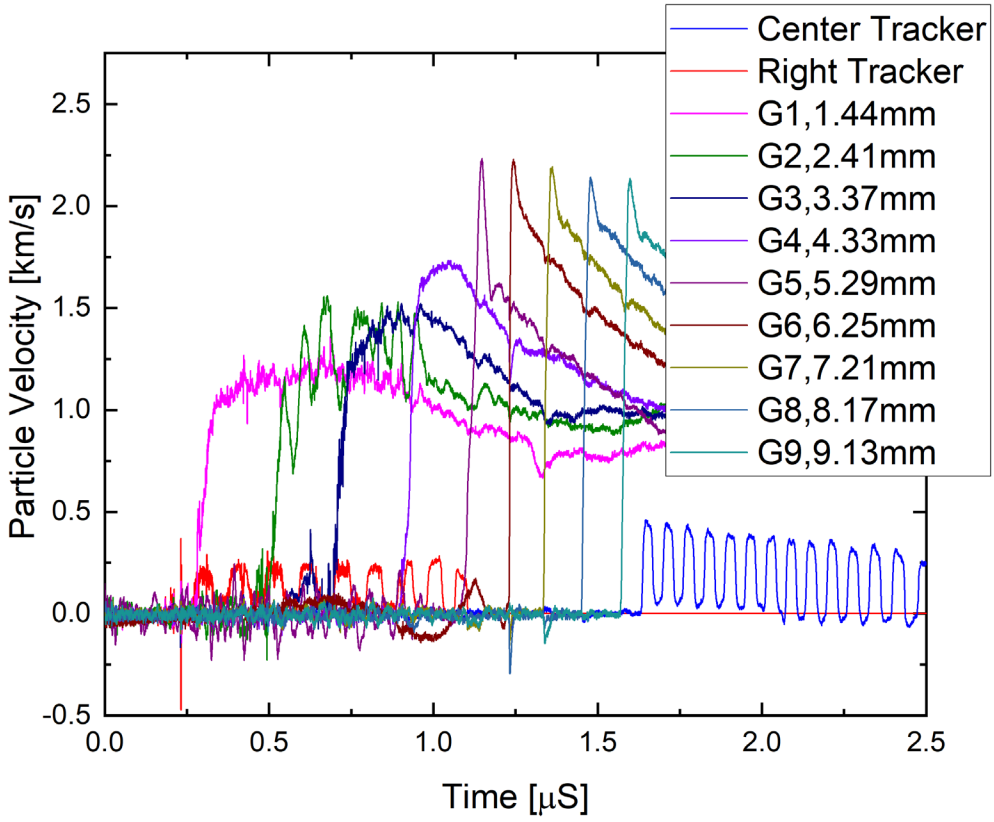

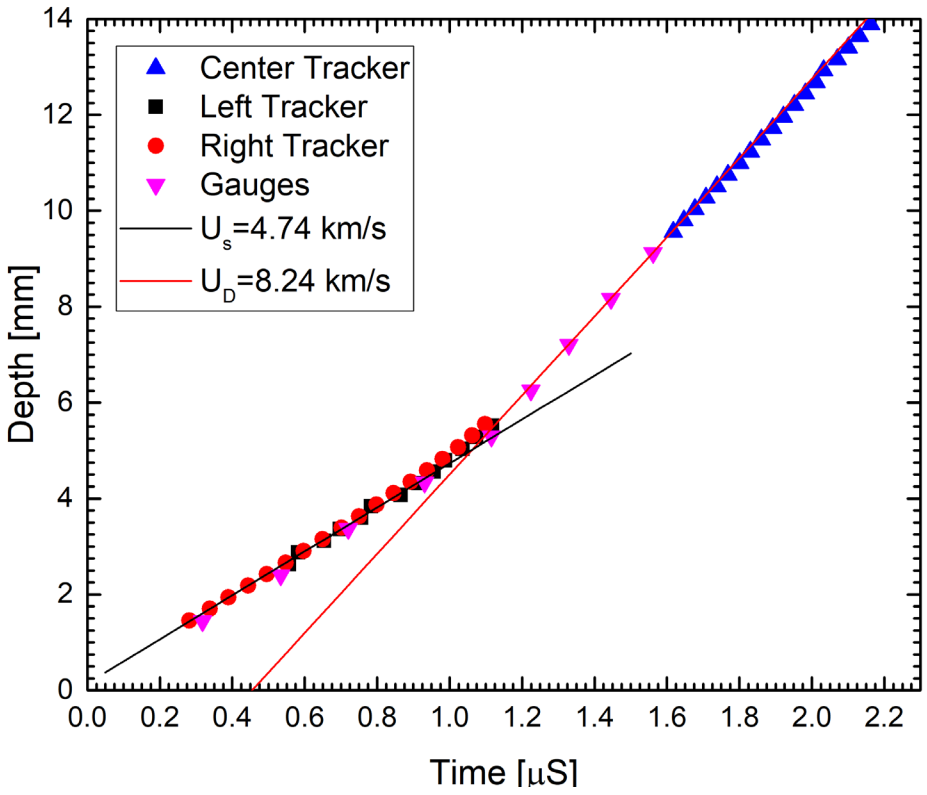

FY19-19

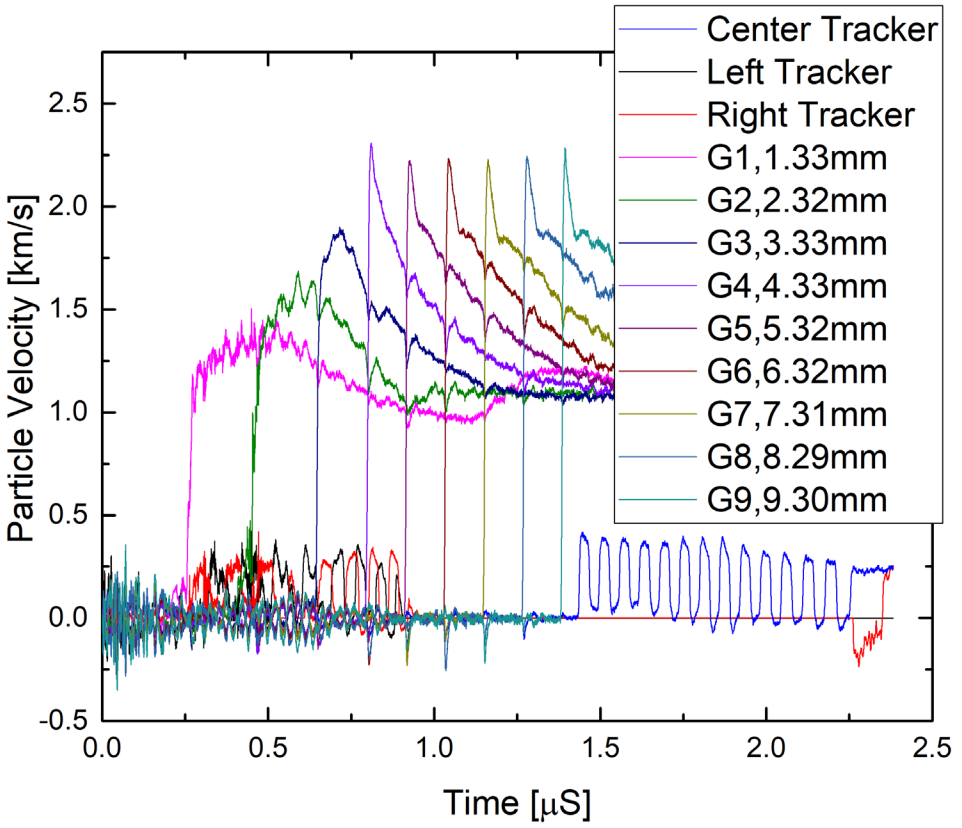

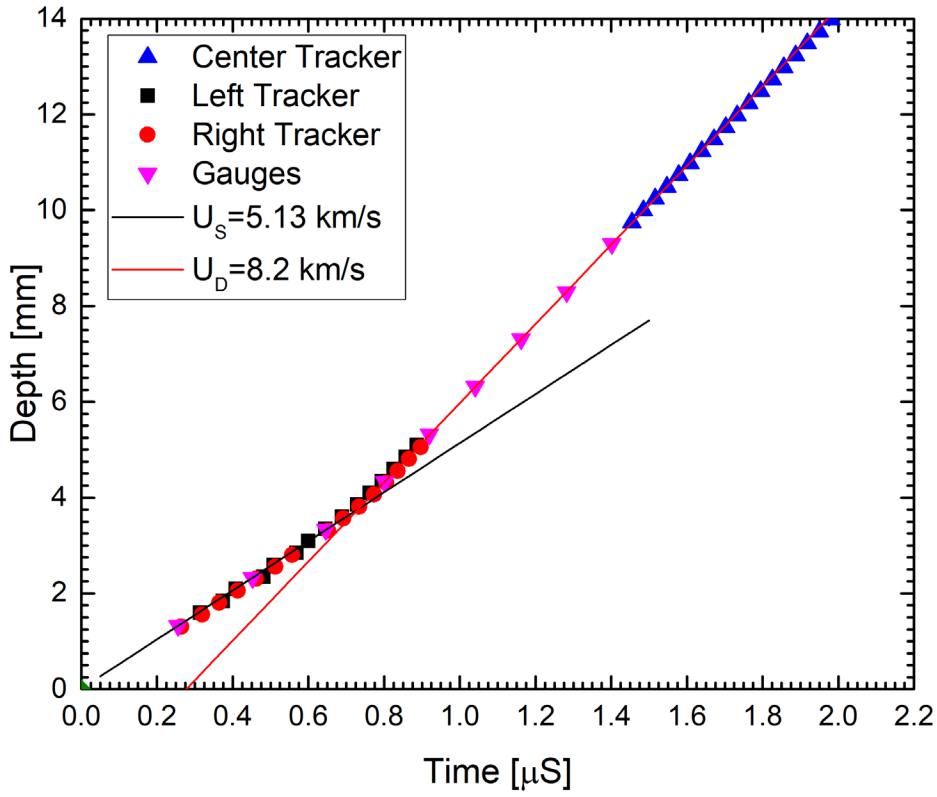

FY19-20

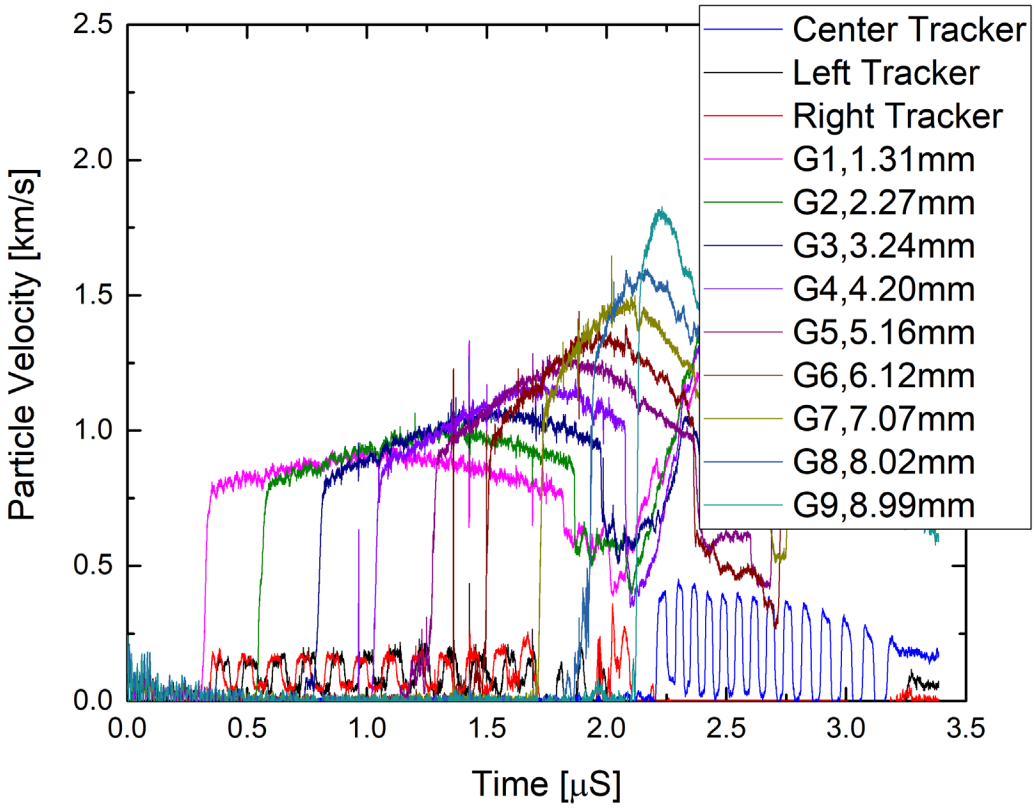

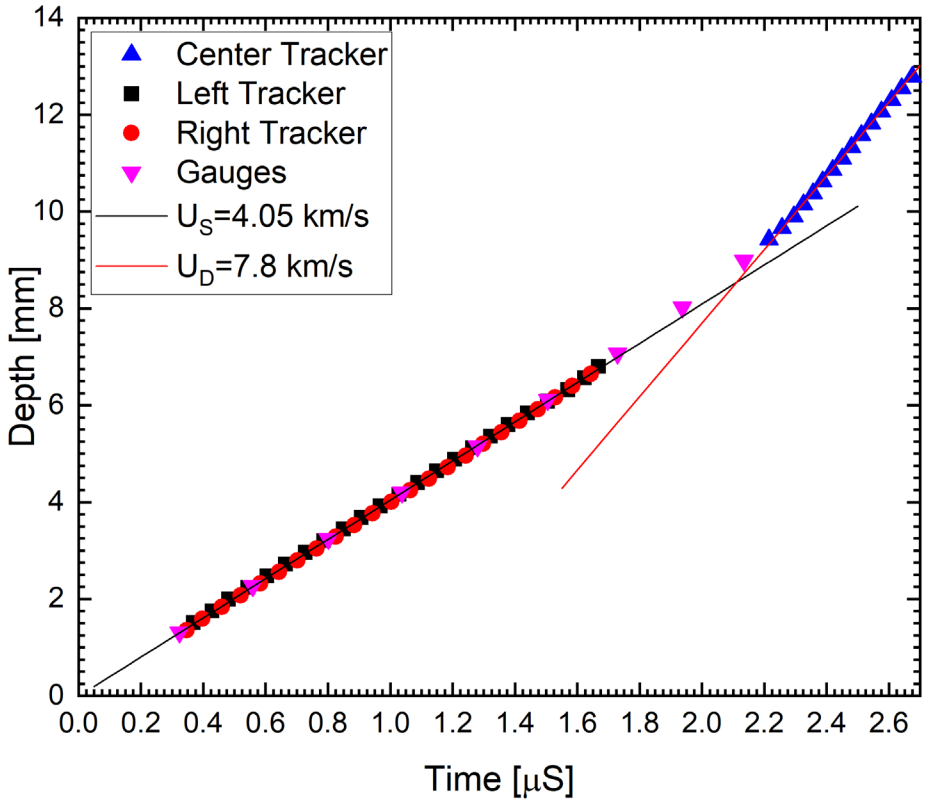

FY20-12

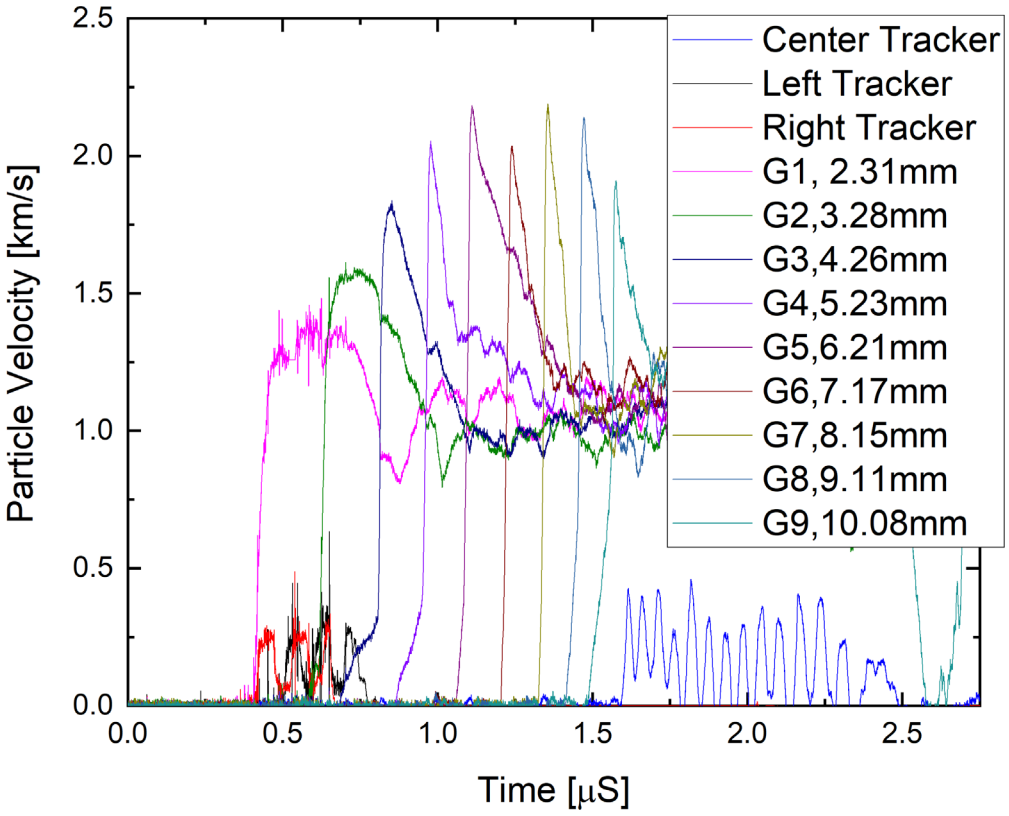

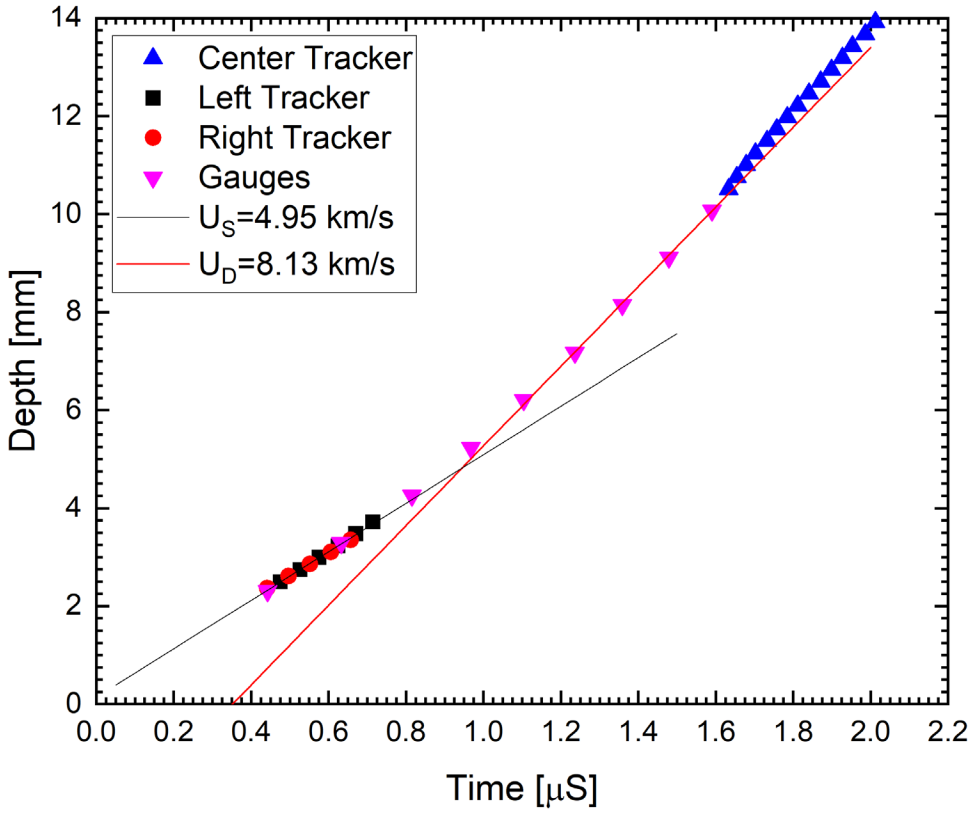

FY20-13

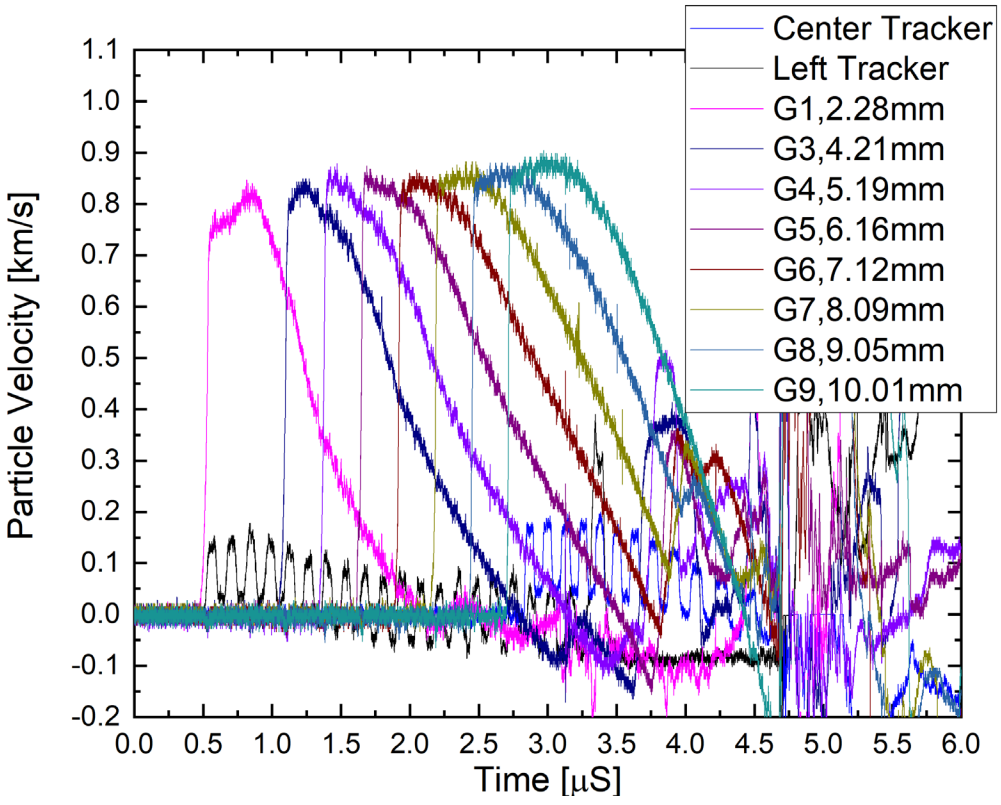

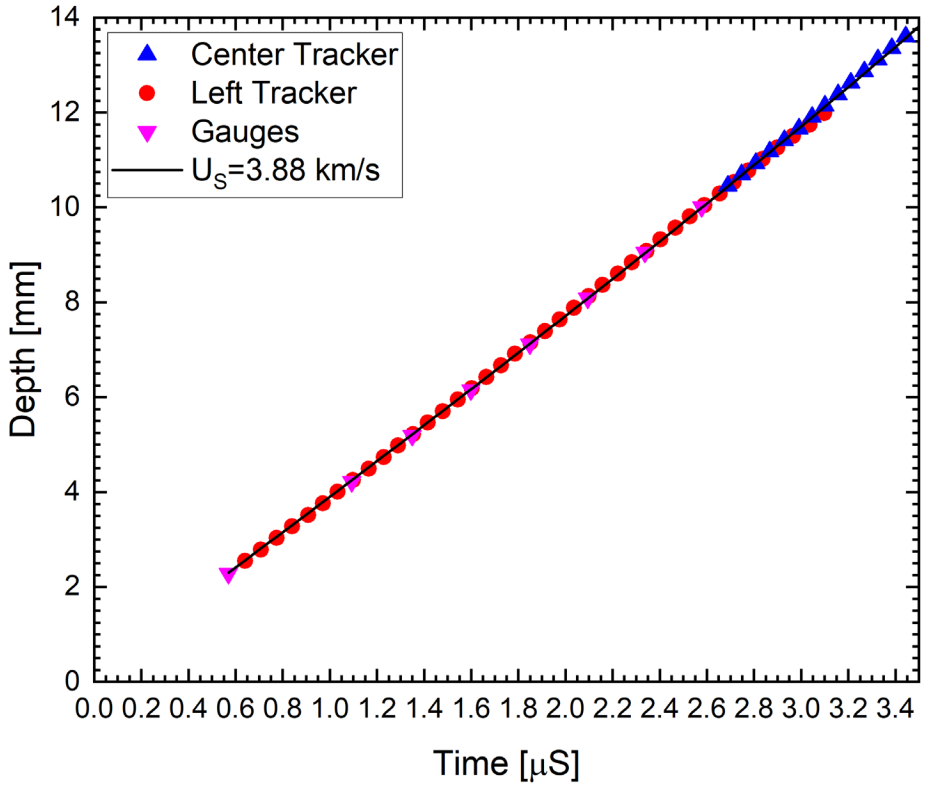

FY20-15

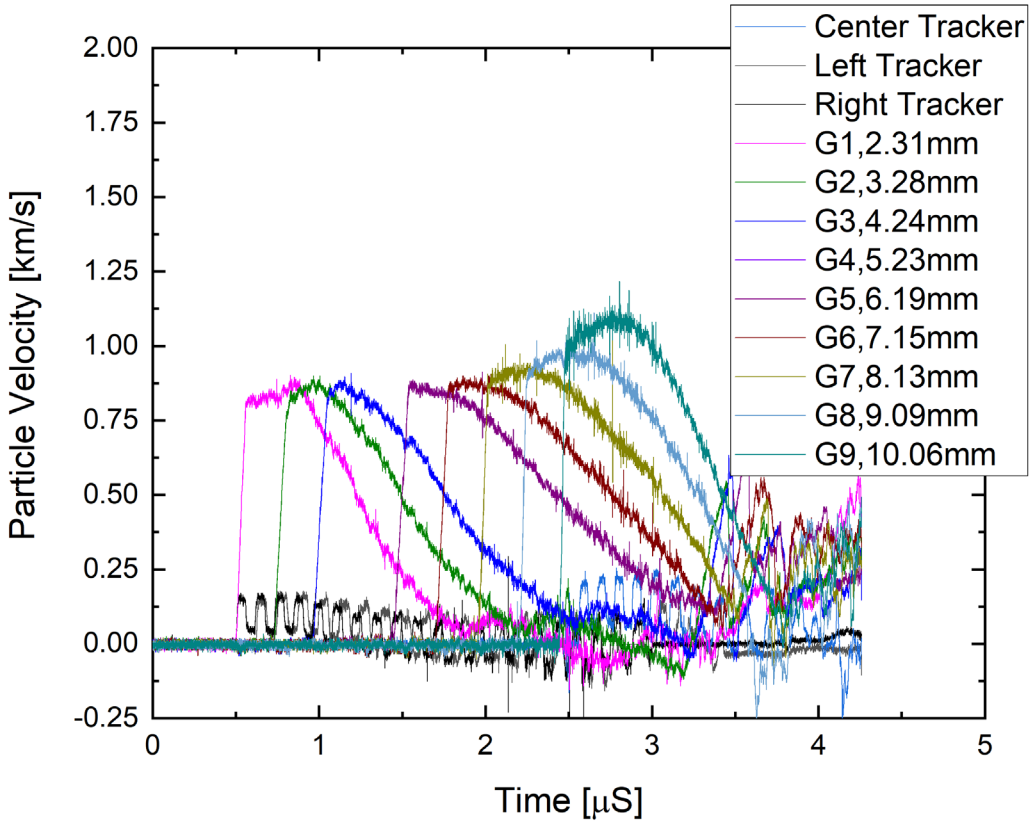

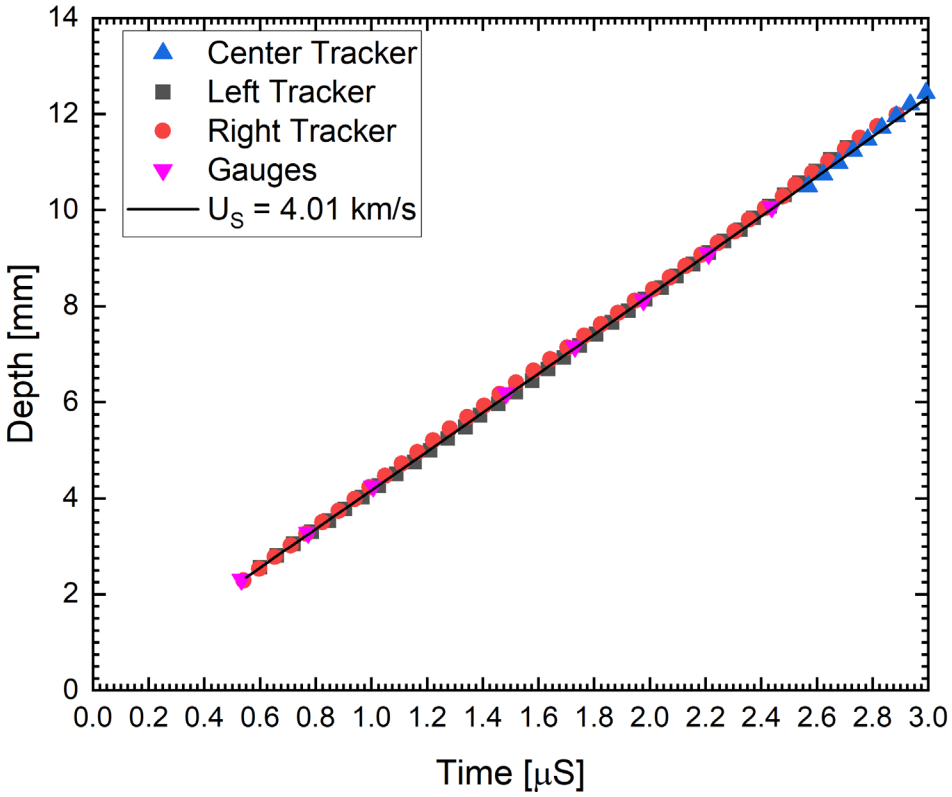

7 REFERENCES

[1] Lee, R., Dorgan, R., Svingala, F., Dattelbaum, D., Furnish, M., and Sutherland, G., "Techniques for the collection and analysis of Pop-plot data for use in parameterization of reactive flow models", AIP Conference Proceedings 1979, 100026 (2018)
[2] Wilde, B., Welle,E., Rumchik,C., "Wedge Test Results and Analysis for PBXN-5, AFRL-RW-EG-TR-2018-052", Air Force Research Laboratory, Eglin AFB, FL, 2018.
[3] Sheffield S.; Gustavsen R.; Alcon R., "In-Situ Magnetic Gauging Technique Used at LANL-Method and Shock Information Obtained," in *Shock Compression of Condensed Matter - 1999*, Snowbird, Utah (2000).
[4] Gustavsen R.; Sheffield S.; Alcon R.; Hill L., "Shock Initiation of New and Aged PBX 9501 Measured with embedded Electromagnetic Particle Velocity Gauges", LA-13634-MS, Los Alamos National Laboratory.
[5] Alcon, R.; Sheffield, S.; Martinez, A.; and Gustavsen, R.,"Magnetic gauge instrumentation on the LANL gas-driven two-stage gun", AIP Conf. Proc. 429, 845 (1998).
[6] Cooper, P.W., Explosives Engineering, Wiley-VCH: New York, 1996, pp 253-319
[7] Howe, P.,"Trends in shock initiation of heterogeneous explosives", LA-UR-98-3026, Los Alamos National Lab.
[8] James, H.,"Critical Energy Criterion for the Shock Initiation of Explosives by Projectile Impact," *Propellants, Explosives, Pyrotechnics ,* no. 13, pp. 35-41, 1988.
[9] James, H., "An Extension to the Critical Energy Criterion Used to Predict Shock Initiation Thresholds," *Propellants, Explosives, Pyrotechnics,* no. 21, pp. 8-13, 1996.
[10] Forbes, J.W., Shock Wave Compression of Condensed Matter: A Primer, Springer-Verlag: New York, 2012,pp 31,59-61
[11] Sutherland, G."Effect of test method on Pop plot results",AIP Conf. Proc. 1426,295-298 (2012).
[12] Schilling, T. and Martin, S., "Shock Initiation of PBXW-113 Using the Wedge Technique," NWCTP 6961, Naval Weapons Center, China Lake, CA, 1988.
[13] Los Alamos data compiled in *LASL Explosive Property Data*, edited by T. R. Gibbs and A. Popolato (University of California Press, Berkeley, 1980).
[14] Gustavsen R.; Sheffield S.; Alcon R.; Hill L.;Winter,R.; Salisbury,D.;and Taylor,P.,"Initiation of EDC-37 measured with embedded electromagnetic particle velocity gauges", AIP Conf. Proc. 505, 879 (2000).
[15] Burns,M. Gustavsen, R., and Bartram, B.," One-dimensional plate impact experiments on the cyclotetramethylene tetranitramine (HMX) based explosive EDC32", J. Appl. Phys. 112, 064910 (2012)
[16] Gustavsen R.; Sheffield S.; and Alcon R.," Measurements of shock initiation in the tri-amino-tri-nitro-benzene based explosive PBX 9502: Wave forms from embedded gauges and comparison of four different material lots", J. Appl. Phys. 99, 114907 (2007).
[17] Neel, C. and Sable, P."Initiation of EXP-A using Large Diameter Flyer Plate Impacts", in preparation.
[18] Burns, M., Gibson, L., Jones, J., Goodbody, A., Dattelbaum, D., and Gustavsen, R.,"One Dimensional shock initiation of hot isostatically pressed composition B", AIP Conference Proceedings 1979, 150007 (2018)
[19] Wilde B., personal communication, 2019

[20] Lacina D. and Neel C., “A high-purity alumina for studies of shock loaded samples”, AIP COnf. Proc. 1979, 030005 (2018)
[21] Unpublished results
[22] Sheffield, S. and Alcon, R.,“In-situ magnetic gauge measurements in Kel-F,” in Shock Compression of Condensed Matter - 1991, edited by S. C. Schmidt, R. D. Dick, J. W. Forbes, and D. G. Tasker (NorthHolland, Amsterdam, The Netherlands, 1991) p. 909.
[23] Neel, C.; Chhabildas, L.; Maines, W.; White, A.; Davis, R.; Vu, D.; and Jamison, K., " AFRL's HP3 60mm Powder Gun, AFRL-RW-EG-TR-2012-098," Air Force Research Laboratory, Eglin AFB, FL, 2015.
[24] Strand,O.; Goosman, D.; Martinez, C.; and Whitworth, T., “Compact system for high-speed velocimetry using heterodyne techniques” Rev. Sci. Instrum. 77, 83108 (2006).
[25] Lacina, D., Neel, C., and Dattelbaum, D., “Shock Response of Poly[methyl methacrylate] (PMMA) Measured with Embedded Electromagnetic Gauges”, *Journal of Applied Physics,* 123(18) 185901.
[26] McQueen, G.; Marsh, S.; Taylor, J.; Fritz, J. and Carter, W.,"The equation of state of solids from shock waves studies," in *High Velocity Impact Phenomena*, New York, Academic, 1970, pg. 230.
[27] James, H. and Lambourn, B.,"On the systematics of particle velocity histories in the shock-to-detonation transition regime," *Journal of Applied Physics,* vol. 100, p. 084906, 2006.